AMERICAN SOCIETY OF CIVIL ENGINEERS

Founded November 5, 1852

TRANSACTIONS

Paper No. 3109
Vol. 126, 1961, Part I

GEOMETRY OF MOIRÉ FRINGES IN STRAIN ANALYSIS

By Stanley Morse,[1] August J. Durelli,[2] and Cesar A. Sciammarella[3]

SYNOPSIS

This paper shows how moiré fringes can be used in the two-dimensional analysis of strains. The fundamental equations of the moiré method are derived and are presented in the form of graphs by means of which strains and rotations can be obtained from simple measurements with a minimum of computation.

INTRODUCTION

The moiré or watered-silk effect is an optical phenomenon produced when two somewhat similar arrays of dots or lines are superimposed, resulting in the formation of alternating light and dark fringes. It is an effect common in everyday life, being seen in mismatched window screens, as the "Venetian-blind" defect in television, and so forth.

Note.—Published essentially as printed here, in August, 1960, in the Journal of the Engineering Mechanics Division, as Proceedings Paper 2576. Positions and titles given are those in effect when the paper or discussion was approved for publication in Transactions.

[1] Assoc. Engr., Mechanics Research Div., Armour Research Foundation, Chicago, Ill.
[2] Prof. of Civ. Engrg., Illinois Inst. of Tech., and Supervisor, Stress Analysis, Armour Research Foundation, Chicago, Ill.
[3] Assoc. Research Engr., Illinois Inst. of Tech., Chicago, Ill.

Because the fringes are the result of displacement of the elements of the two arrays with respect to each other, the moiré effect is obviously a tool by which strain measurements can be made. If, for example, one begins with two identical sets of straight, parallel lines, fringes are produced by either rotation (Fig. 1(a)) or elongation (Fig. 1(b)) of one set with respect to the other.

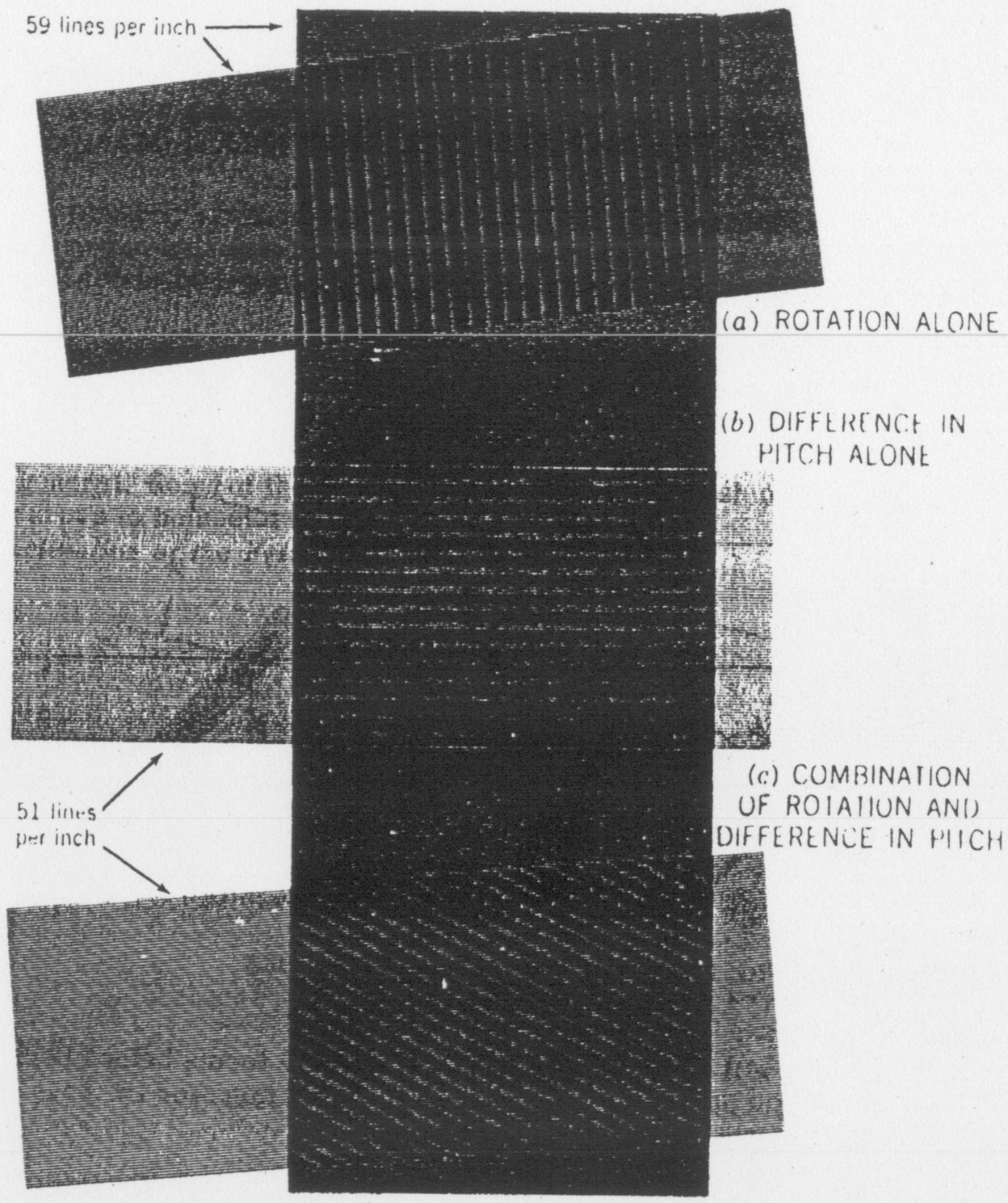

FIG. 1.—MECHANISM OF FORMATION OF MOIRÉ FRINGES

Simple equations govern the interpretation of pure rotations and elongations. Within the limits of small deformations, these effects can be considered to be linear and capable of being superimposed. A number of papers have been published under these assumptions, notably by R. Weller and M. Shepard[4] and by P. Dantu.[5]

[4] "Displacement Measurements by Technical Interferometry," by R. Weller and B. M. Shepard, Proceedings, S.E.S.A., No. 1, 1948.
[5] "Utilization des Reseau pour l'Etude des Deformations," by P. Dantu, Laboratoire Central des Ponts et Chaussees, Paris, Publication 57-6, 1957.

Actually, the moiré effect is not limited in any way to separate rotations and elongations nor to infinitesimal deformations. Neither is it necessary that the arrays be originally identical in either spacing or orientation.

In this paper only sets of straight, parallel, nondiffracting lines will be considered. However, moiré fringes that can be analyzed could be obtained from circular, radial, or other nonparallel arrays, and diffraction gratings could be used under suitable conditions.

Fig. 1(c) shows the effect of combined rotation and differences in pitch of straight, parallel sets of lines representing a homogeneous field for which equations will be derived. The relationships so obtained can also be applied to sufficiently small elements of a nonhomogeneous field such as would be presented in a general two-dimensional strain problem.

The moiré method can certainly be used for the analysis of large strains and rotations, but such application is beyond the scope of this paper. However, the equations will be derived in the most general terms before being related to such specific quantities as strain. Approximations for the case of infinitesimal deformations will also be developed.

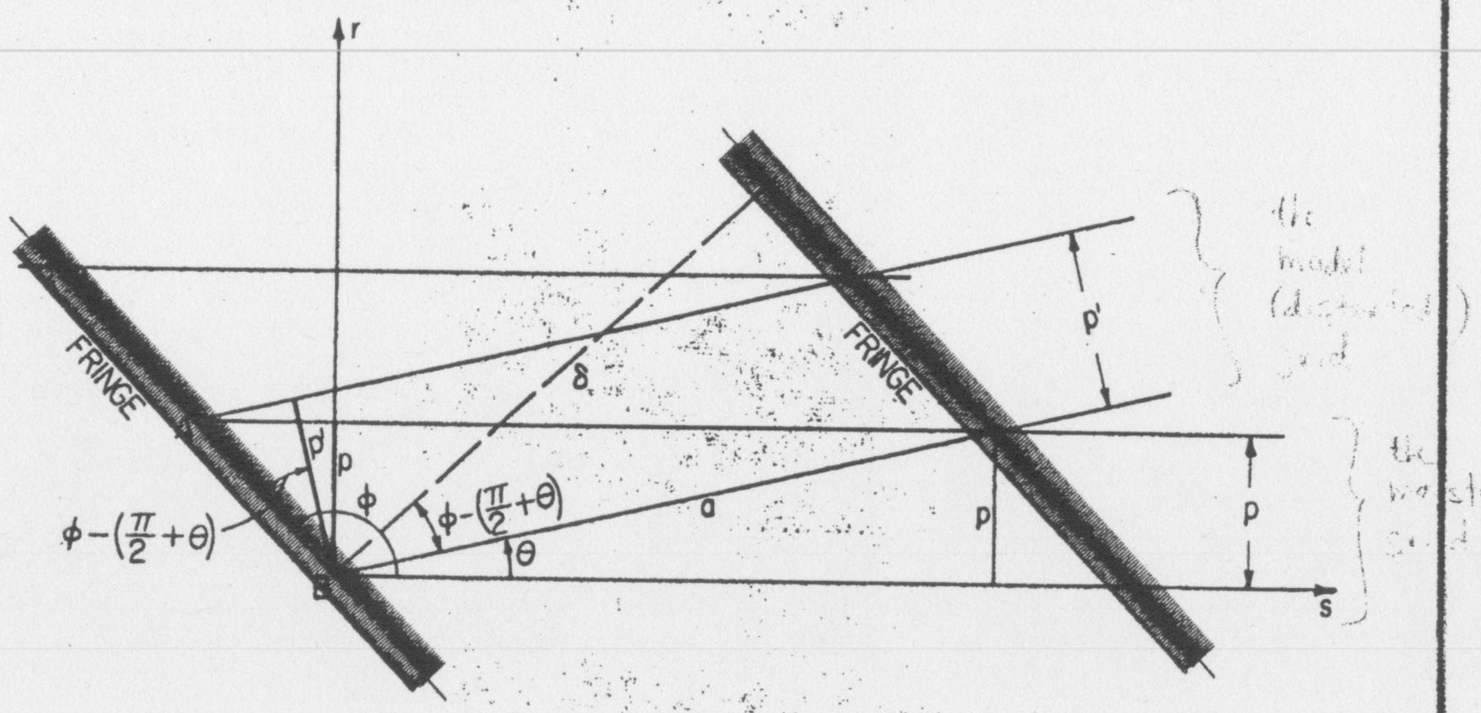

FIG. 2.—GEOMETRY OF MOIRÉ FRINGES

BASIC PROPERTIES AND DEFINITIONS

In the subsequent derivations, a fixed array of straight, parallel lines called the "master grid" is used as a reference both for analysis of the properties of the moiré and for establishment of coordinate directions. The center-to-center distance between the master grid lines is defined as the master pitch, p, and the directions perpendicular and parallel to these lines are designated as r and s, respectively.

The model also bears a similar array of lines which in the undistorted state are not necessarily of the same pitch as the master grid. The pitch of this grid at any particular point in any state of distortion is called the "model pitch" and is designated by p'.

The angle θ is defined as the acute angle at any point and in any given state of deformation measured from the fixed master grid lines to the model grid lines. The angle from the fixed master grid lines to a fringe at a point measured in the same direction as θ is designated as ϕ and may be either acute or obtuse. Fig. 2 shows how to obtain the inclination ϕ of the moiré fringes and their distances δ as functions of the master grid pitch p, the model grid pitch p', and the rotation θ of both grids at a point.

Let us assume either the case of a homogeneous deformation and rotation (which may be accompanied by translation) or of a sufficiently small element of a nonhomogeneous field. Equations relating any desired sets of parameters for the moiré phenomenon are easily derived from the simple geometry of fringe formation. Those for the normal fringe spacing, δ, and the fringe angle, ϕ, are perhaps the most fundamental. However, the information available for the analysis will usually be in the form of photographs on which δ and ϕ and the coordinate fringe spacings δ_r and δ_s can be measured, and the purpose of the analysis will be the determination of θ and p' at the desired points. Obviously, the master grid pitch, p , and the direction of its lines must be known.

Several of the expressions developed herewith can be obtained in other ways, some by using the property of moiré fringes of being loci of points of equal displacement. The derivations that follow, however, are very simple and general. Some of the curves representing relationship between parameters may prove to be useful in practice.

Inclination of the Fringes.

$$\overline{AB} = \frac{P}{\cos\left(\phi - \frac{\pi}{2}\right)} = \frac{P}{\sin\phi} \quad \ldots\ldots\ldots\ldots\ldots\ldots (1)$$

and

$$\overline{AB} = \frac{p'}{\cos\left(\phi - \frac{\pi}{2} - \theta\right)} = \frac{p'}{\sin(\phi - \theta)} \quad \ldots\ldots\ldots\ldots\ldots\ldots (2)$$

therefore

$$p' = p\,\frac{\sin(\phi - \theta)}{\sin\phi} \quad \ldots\ldots\ldots\ldots\ldots\ldots (3)$$

Because

$$p\,(\sin\phi\cos\theta - \sin\theta\cos\phi) = p'\sin\phi \quad \ldots\ldots\ldots\ldots (4)$$

then

$$\tan\phi = \frac{p\sin\theta}{p\cos\theta - p'} \quad \ldots\ldots\ldots\ldots\ldots\ldots (5)$$

Distance between Fringes.—Also from Fig. 2 and the foregoing:

$$a = \frac{p}{\sin\theta} \quad \ldots\ldots\ldots\ldots\ldots\ldots (6)$$

and

$$\delta = a\cdot\cos\left(\phi - \frac{\pi}{2} - \theta\right) = \frac{p\sin(\phi - \theta)}{\sin\theta} = \frac{p'\sin\phi}{\sin\theta} \quad \ldots\ldots\ldots (7)$$

From Eq. 5:

$$\sin \phi = \frac{p \sin \theta}{\sqrt{p^2 \sin^2 \theta + (p \cos \theta - p')^2}} \quad \ldots\ldots\ldots (8)$$

and

$$\delta = \frac{p\, p'}{\sqrt{p^2 \sin^2 \theta + (p \cos \theta - p')^2}} \quad \ldots\ldots\ldots (9)$$

Rotation in Terms of the Inclination of the Fringes and their Spacing.—From Eq. 7:

$$\frac{\delta}{p} \sin \theta = \sin (\phi - \theta) = \sin \phi \cos \theta - \cos \phi \sin \theta \quad \ldots\ldots (10)$$

and

$$\tan \theta = \frac{\sin \phi}{\frac{\delta}{p} + \cos \phi} \quad \ldots\ldots\ldots\ldots\ldots (11)$$

To represent graphically the relationship between θ and ϕ it is convenient to introduce the following definitions:

$$\alpha_\delta = \frac{\delta}{p} \tan \theta = \frac{\delta}{p}\left[\frac{\sin \phi}{\frac{\delta}{p} + \cos \phi}\right] = \frac{\sin \phi}{1 + \frac{p}{\delta} \cos \phi} \quad \ldots\ldots\ldots (12)$$

and

$$\tan \theta = \alpha_\delta \frac{p}{\delta} \quad \ldots\ldots\ldots\ldots\ldots (13)$$

Values of α_δ for the entire possible range of ϕ (0° to 180°) and for various values of δ/p are plotted in Fig. 3, permitting easy determination of the model rotation at a point without knowledge of p', the model pitch.

Model Pitch in Terms of ϕ and δ.—Again, from Eq. 7:

$$p' = \frac{\delta \sin \theta}{\sin \phi} \quad \ldots\ldots\ldots\ldots\ldots (14)$$

From Eq. 11:

$$\sin \theta = \frac{\sin \phi}{\sqrt{\sin^2 \phi + \left(\frac{\delta}{p} + \cos \phi\right)^2}} \quad \ldots\ldots\ldots (15)$$

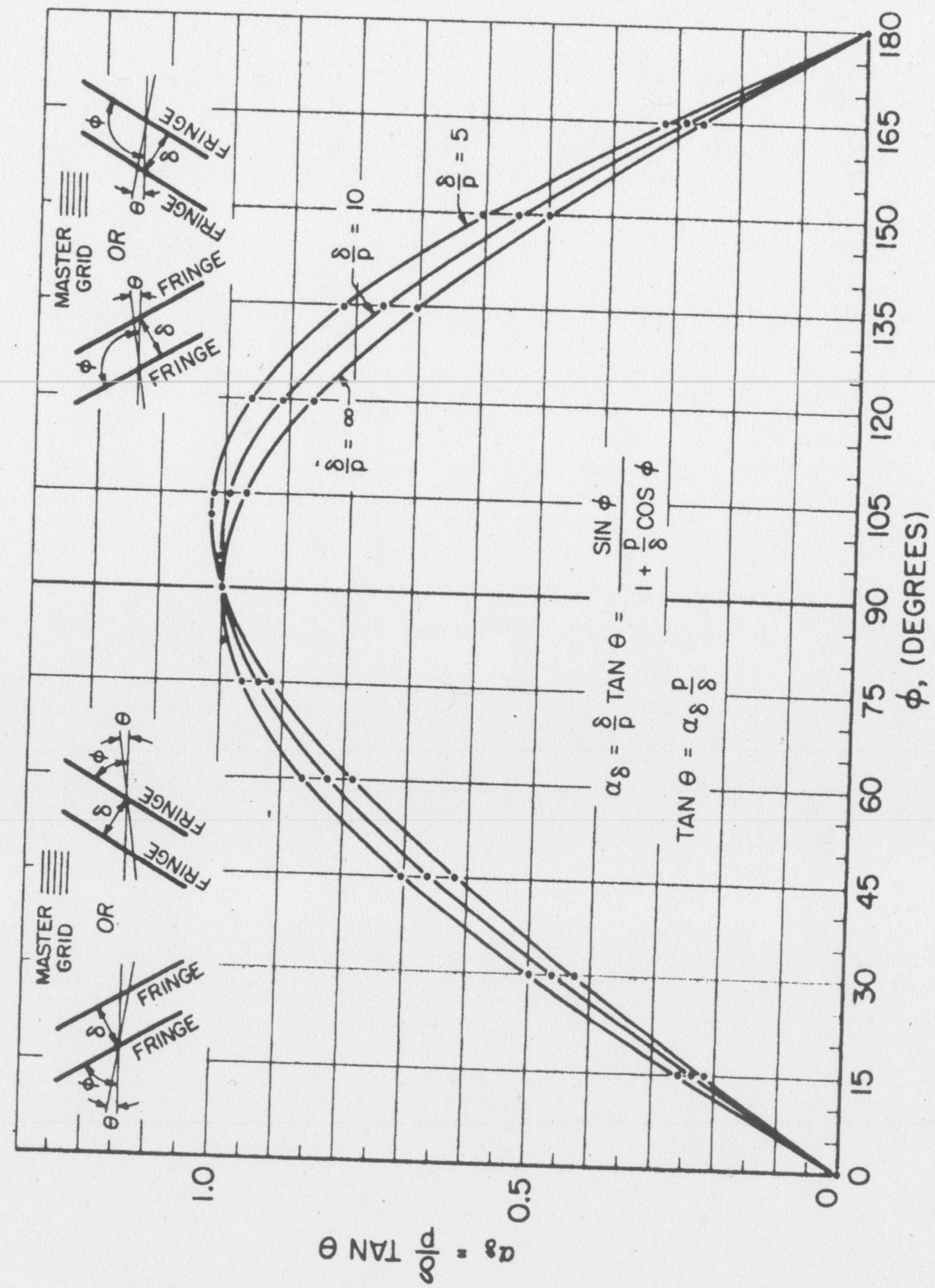

FIG. 3.—ROTATION AS A FUNCTION OF FRINGE ANGLE AND NORMAL FRINGE SPACING

$$p' = \frac{\delta}{\sqrt{1 + \left(\frac{\delta}{p}\right)^2 + 2\left(\frac{\delta}{p}\right)\cos\phi}} \quad \ldots\ldots\ldots\ldots (16)$$

and

$$\frac{p}{p'} = \sqrt{\left(\frac{p}{\delta}\right)^2 + 2\left(\frac{p}{\delta}\right)\cos\phi + 1} \quad \ldots\ldots\ldots\ldots (17)$$

Determination of "True" and "Conventional" Strains.—To compute the value of the strain using the measured quantities δ and ϕ, a graphical construction can be utilized. For this construction it is convenient to introduce the following definitions:

$$\beta_\delta = \frac{\delta}{p}\left(1 - \frac{p}{p'}\right) = \frac{\delta}{p}\left[1 - \sqrt{\left(\frac{p}{\delta}\right)^2 + 2\left(\frac{p}{\delta}\right)\cos\phi + 1}\right] \ldots\ldots (18)$$

and

$$\epsilon_{r\ true} = 1 - \frac{p}{p'} = \frac{p' - p}{p'} = \beta_\delta\left(\frac{p}{\delta}\right) \quad \ldots\ldots\ldots\ldots (19)$$

Values of β_δ for all possible values of ϕ and for various values of δ/p have been plotted in Fig. 4, permitting easy determination of the model pitch, pitch ratio, or the quantity $1 - (p/p')$ free from the influence of rotation. It should be noted that $1 - (p/p')$ is the "true" strain perpendicular to the direction of the master grid lines if p and p' were originally equal before distortion of the model.

If Eq. 19 is converted to the form:

$$\epsilon_r = \frac{p'}{p} - 1 = \frac{p' - p}{p} = \frac{\frac{\beta_\delta\, p}{\delta}}{1 - \frac{\beta_\delta\, p}{\delta}} \quad \ldots\ldots\ldots\ldots (20)$$

we obtain the "conventional" or "nominal" strain perpendicular to the direction of the master grid lines.

Rotation in Terms of ϕ and Distance between Fringes along the Coordinate Directions.—In many cases it may be preferred to measure the fringe spacing along the coordinate directions or it may be desirable to have a second method for checking the model rotations. From Fig. 5 we have, for the two cases (a) ϕ acute, and (b) ϕ obtuse, respectively:

$$\delta = \delta_s \sin\phi \quad \ldots\ldots\ldots\ldots\ldots\ldots (21a)$$

and

$$\delta = \delta_s \sin(\pi - \phi) = \delta_s \sin\phi \quad \ldots\ldots\ldots\ldots (21b)$$

Substituting Eqs. 21 into Eq. 11 and extracting $\sin\theta$ by trigonometric transformation, we obtain:

$$\sin\theta = \frac{1}{\sqrt{1 + \left(\frac{\delta_s}{p} + \cot\phi\right)^2}} \quad \ldots\ldots\ldots\ldots (22)$$

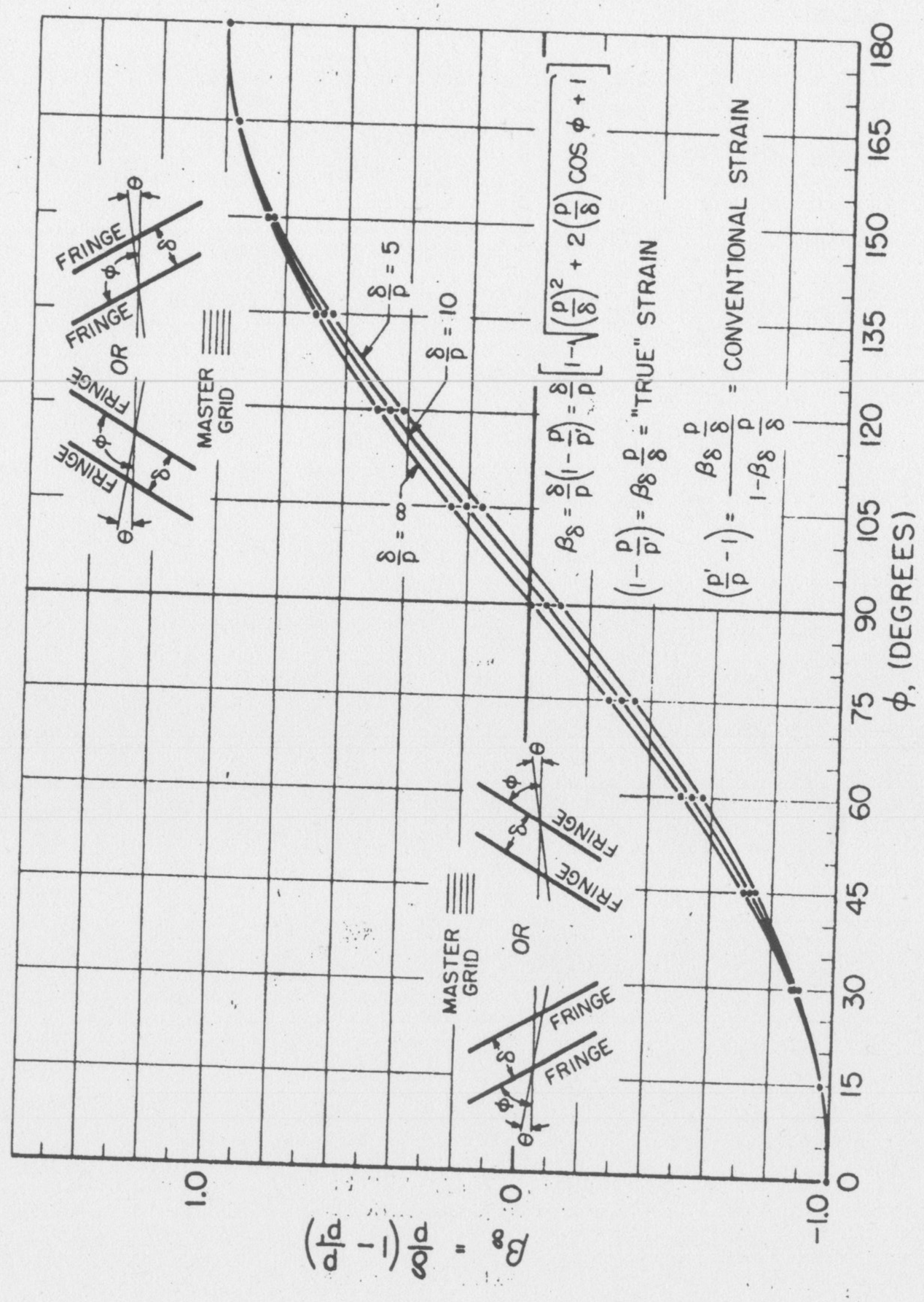

FIG. 4.—MODEL PITCH AS A FUNCTION OF FRINGE ANGLE AND NORMAL FRINGE SPACING

Similarly, from Fig. 5:

$$\delta = \delta_r \cos \phi \quad \ldots\ldots\ldots\ldots\ldots\ldots\ldots\ldots \quad (23a)$$

$$\delta = \delta_r \cos (\pi - \phi) = \delta_r (- \cos \phi) \quad \ldots\ldots\ldots\ldots \quad (23b)$$

To avoid having to give a negative sign to δ_r, a measured distance, these equations can be combined as:

$$\delta = \delta_r \mid \cos \phi \mid \quad \ldots\ldots\ldots\ldots\ldots\ldots\ldots \quad (24)$$

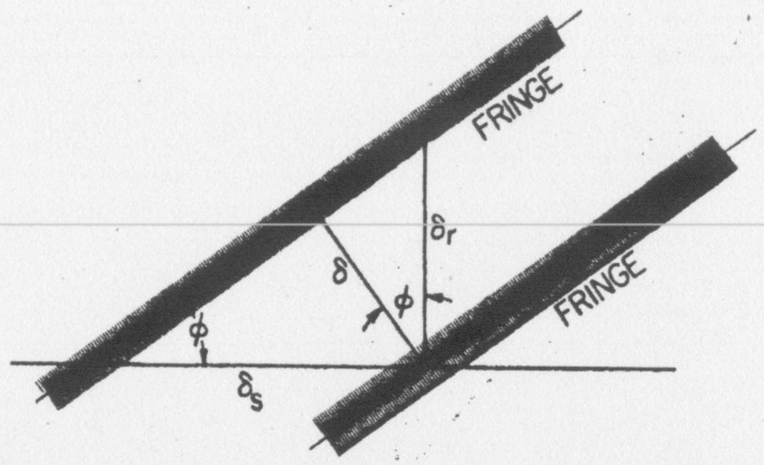

CASE (a), ϕ AN ACUTE ANGLE

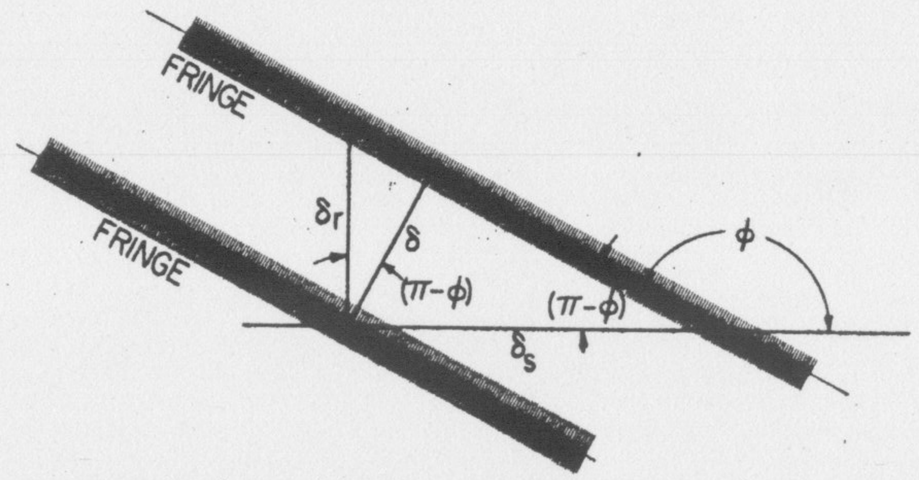

CASE (b), ϕ AN OBTUSE ANGLE

FIG. 5.—SKETCHES TO DERIVE THE FRINGE SPACING IN THE COORDINATE DIRECTIONS

Again substituting in Eq. 11 and extracting sin θ:

$$\sin \theta = \frac{1}{\sqrt{1 + \left(1 + c \frac{\delta_r}{p}\right)^2 \cot^2 \phi}} \quad \ldots\ldots\ldots\ldots \quad (25)$$

where $c = +1$, $0 < \phi < \frac{\pi}{2}$ and $c = -1$, $\frac{\pi}{2} < \phi < \pi$.

Following the same method used previously we can define α_s and α_r as follows:

$$\alpha_s = \frac{\delta_s}{p} \sin \theta = \frac{\frac{\delta_s}{p}}{\sqrt{1 + \left(\frac{\delta_s}{p} + \cot \phi\right)^2}} \quad \ldots\ldots\ldots \quad (26)$$

and

$$\alpha_r = \frac{\delta_r}{p} \sin \theta = \frac{\frac{\delta_r}{p}}{\sqrt{1 + \left(1 + c \frac{\delta_r}{p}\right)^2 \cot^2 \phi}} \quad \ldots\ldots\ldots \quad (27)$$

Then

$$\sin \theta = \alpha_s \frac{p}{\delta_s} \quad \ldots\ldots\ldots\ldots\ldots\ldots \quad (28)$$

and

$$\sin \theta = \alpha_r \frac{p}{\delta_r} \quad \ldots\ldots\ldots\ldots\ldots\ldots \quad (29)$$

Values of α_s and α_r are plotted in Figs. 6 and 7, respectively. Their combined usable ranges cover all possible values of ϕ.

Model Pitch in Terms of ϕ and Distances between Fringes along the Coordinate Directions.—Substituting Eq. 24 into Eq. 17 and setting up a relationship similar to Eq. 18 we can define:

$$\beta_r = \frac{\delta_r}{p} \left(1 - \frac{p}{p'}\right) \quad \ldots\ldots\ldots\ldots\ldots\ldots\ldots\ldots \quad (30a)$$

and

$$\beta_r = \frac{\delta_r}{p} \left[1 - \sqrt{\left(\frac{p}{\delta_r}\right)^2 \frac{1}{\cos^2 \phi} + 2c \frac{p}{\delta_r} + 1}\right] \quad \ldots\ldots\ldots \quad (30b)$$

in which $c = +1$, $0 < \phi < \pi/2$ and $c = -1$, $\pi/2 < \phi < \pi$.

Similarly, substituting Eqs. 21 into Eq. 17:

$$\beta_s = \frac{\delta_s}{p} \left(1 - \frac{p}{p'}\right) \quad \ldots\ldots\ldots\ldots\ldots\ldots\ldots\ldots \quad (31a)$$

and

$$\beta_s = \frac{\delta_s}{p} \left[1 - \frac{1}{\sin \phi} \sqrt{\left(\frac{p}{\delta_s}\right)^2 + \frac{p}{\delta_s} \sin 2\phi + \sin^2 \phi}\right] \quad \ldots\ldots \quad (31b)$$

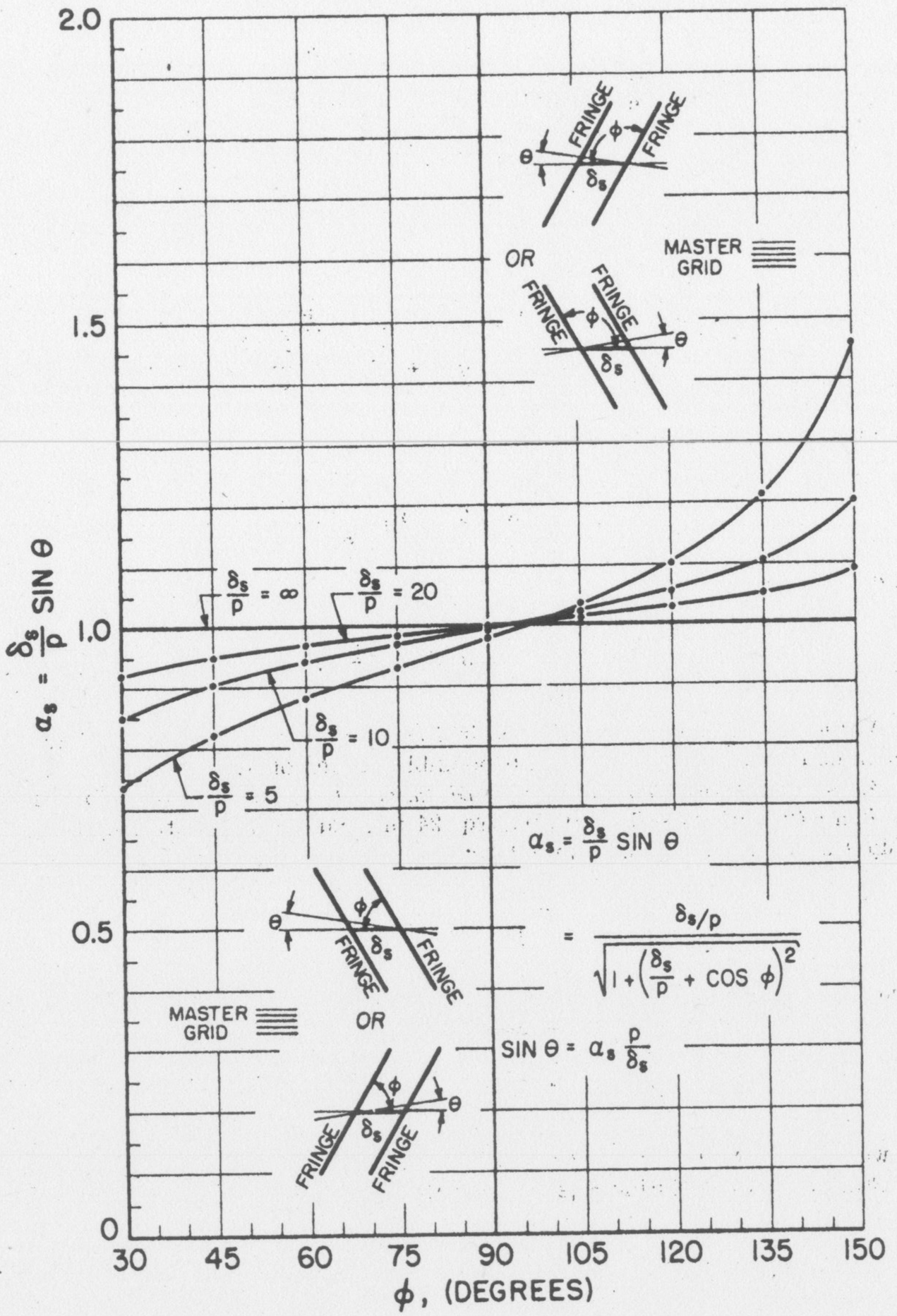

FIG. 6.—ROTATION AS A FUNCTION OF FRINGE ANGLE AND FRINGE SPACING IN THE DIRECTION OF THE MASTER GRID LINES

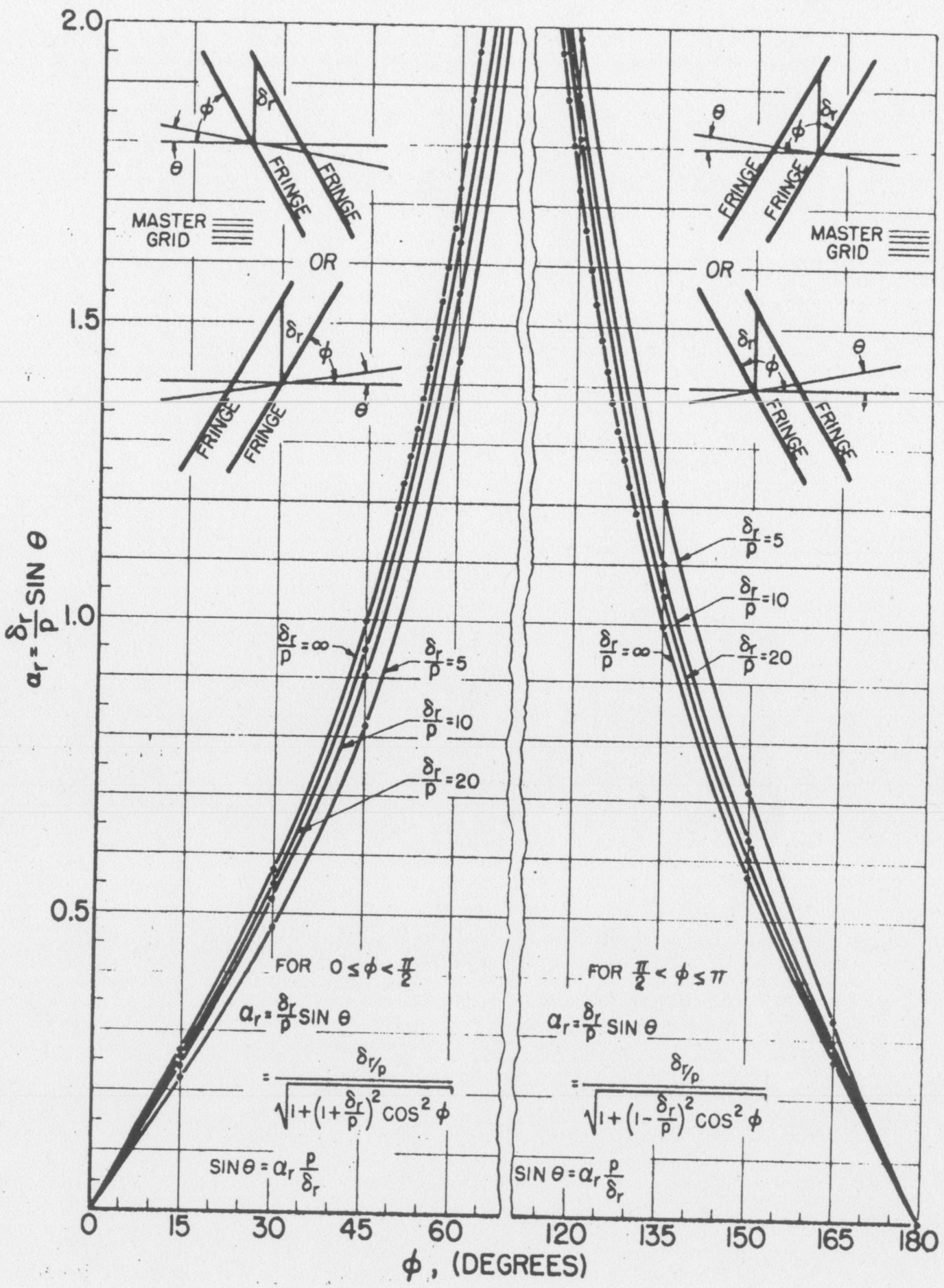

FIG. 7.—ROTATION AS A FUNCTION OF FRINGE ANGLE AND FRINGE SPACING NORMAL TO THE DIRECTION OF THE MASTER GRID LINES

Then:

$$\epsilon_{r\ true} = 1 - \frac{p}{p'} = \frac{p' - p}{p'} = \beta_r \left(\frac{p}{\delta_r}\right) \quad \ldots\ldots\ldots\ldots (32)$$

and

$$1 - \frac{p}{p'} = \beta_s \left(\frac{p}{\delta_s}\right) \quad \ldots\ldots\ldots\ldots\ldots\ldots (33)$$

Values of β_r and β_s are plotted in Figs. 8 and 9, respectively. Their combined usable ranges cover all possible values of ϕ.

Simplified Equations for Small Deformations and Rotations.—It is apparent from Fig. 8 that if ϕ is sufficiently close to 0° or 180° (depending also on the value of δ_r/p), the value of β_r is close to -1.0 or 1.0. This means that rotations θ are very small (Eq. 11). In many problems, sufficient accuracy may result from taking $\beta_r = \pm 1$ and reducing Eq. 32 to:

$$\epsilon_{true} = \frac{p' - p}{p'} = \pm \frac{p}{\delta_r} \quad \ldots\ldots\ldots\ldots\ldots (34)$$

By simple transformation

$$\epsilon_{nom} = \frac{p' - p}{p} = \frac{\pm \frac{p}{\delta_r}}{1 \mp \frac{p}{\delta_r}} \quad \ldots\ldots\ldots\ldots\ldots (35)$$

If, furthermore, p/δ_r is sufficiently small in comparison with unity (that is if strains are very small), Eqs. 34 and 35 both reduce to:

$$\epsilon = \pm \frac{p}{\delta_r} \quad \ldots\ldots\ldots\ldots\ldots\ldots (36)$$

On the other hand, in Fig. 6, if ϕ is sufficiently close to 90° (depending on the value of δ_s/p) the value of α_s is close to 1.0, and sufficient accuracy may result from a reduction of Eq. 29 to

$$\sin \theta = \frac{p}{\delta_s} \quad \ldots\ldots\ldots\ldots\ldots\ldots (37)$$

Determination of the Direction of the Fringe Angle.—In order to determine the direction in which the fringe angle, ϕ, is to be measured in the foregoing equations and graphs, a small amount of information is needed in addition to a photograph of the fringe pattern. For example, the direction of rotation may often be deduced from the loading conditions or could always be found by means of a coarse set of lines or dots on the model in addition to the closely-spaced array which produces the moiré. Once the direction of θ is known, the direction of ϕ is determined by its definition and all ambiguity disappears.

Alternatively, all ambiguity is removed if the sign of the quantity $1-(p/p')$ is known, that is, whether p/p' is greater or less than unity. This can usually

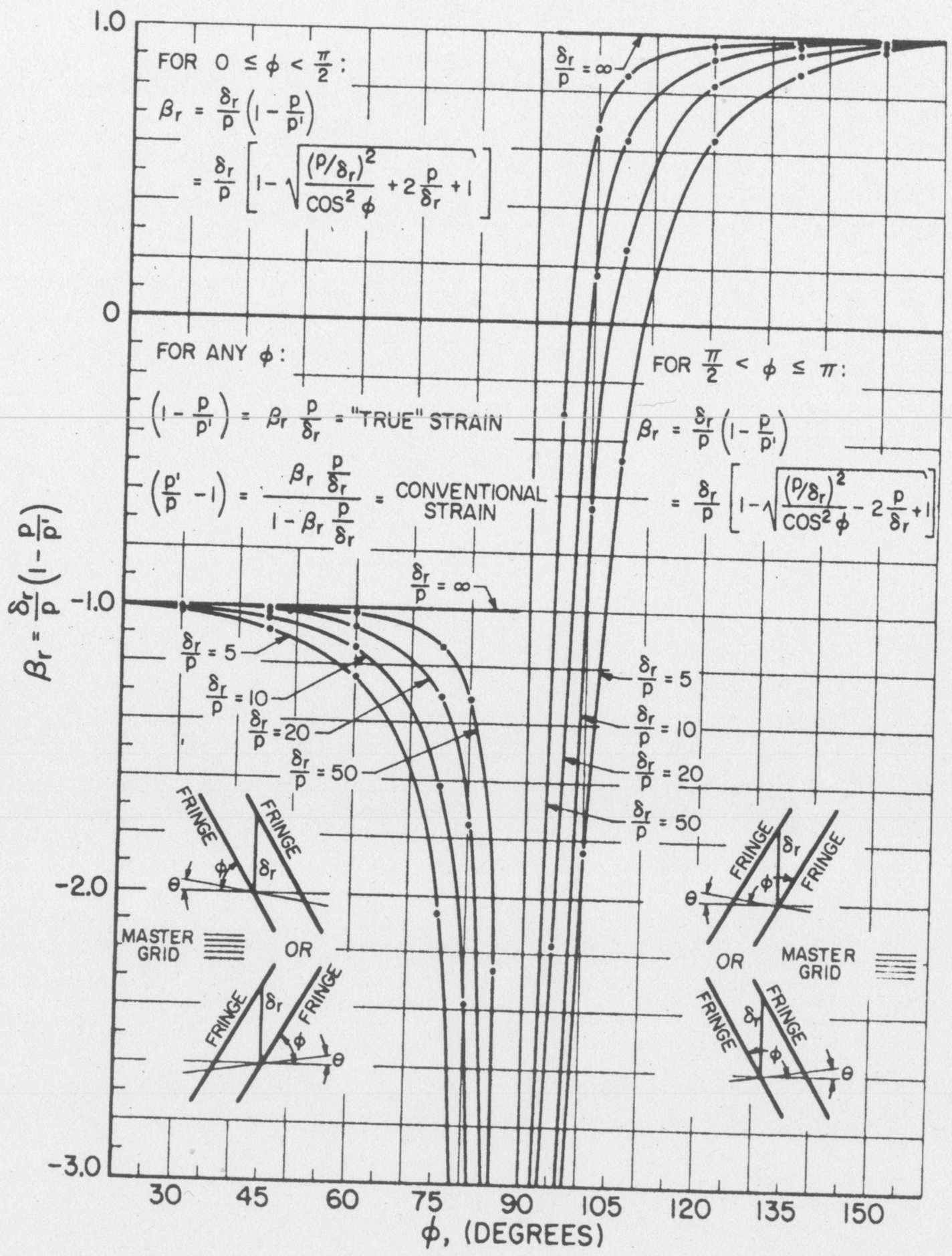

FIG. 8.—MODEL PITCH AS A FUNCTION OF FRINGE ANGLE AND FRINGE SPACING PERPENDICULAR TO THE DIRECTION OF THE MASTER GRID LINES

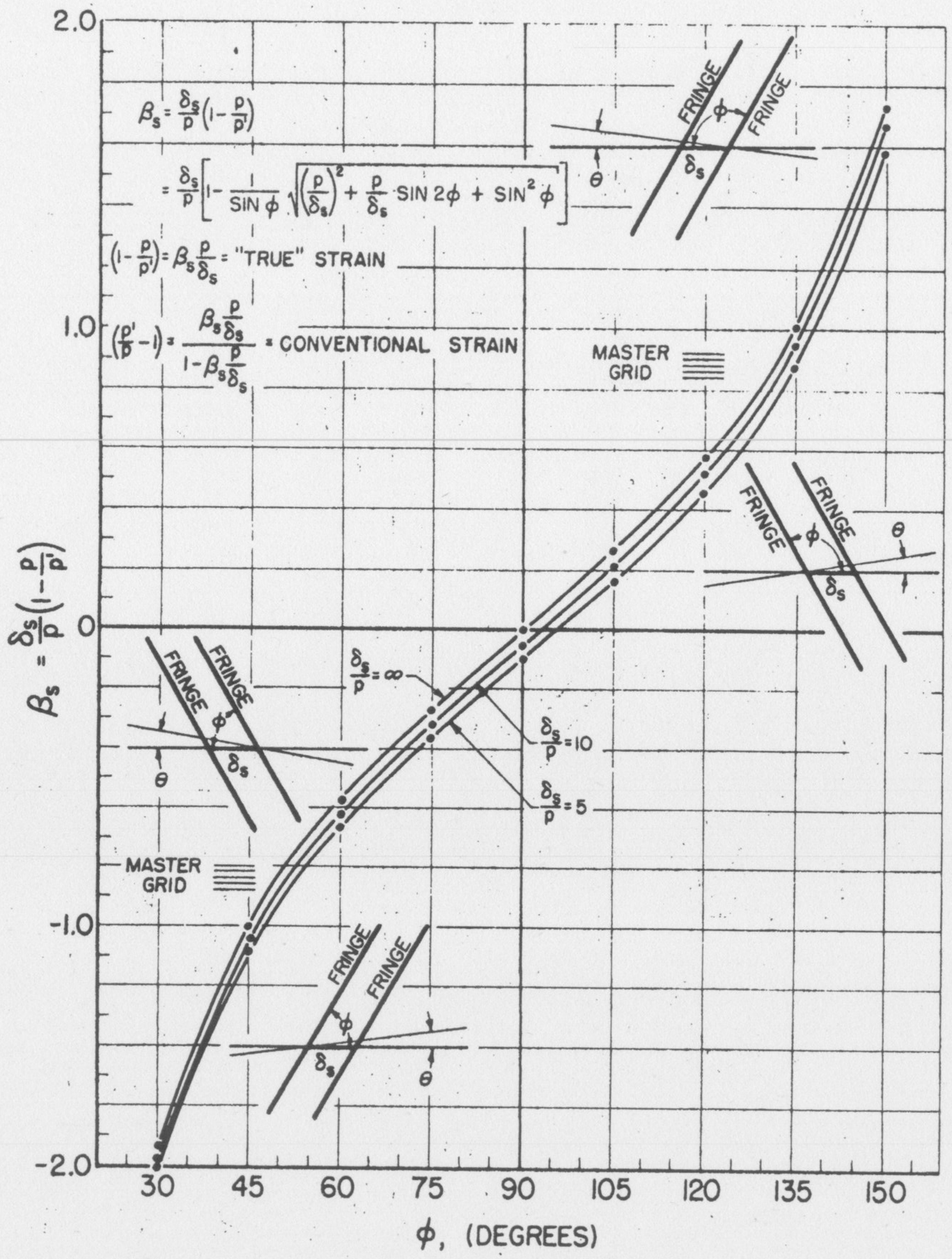

FIG. 9.—MODEL PITCH AS A FUNCTION OF THE FRINGE ANGLE AND FRINGE SPACING IN THE DIRECTION OF THE MASTER GRID LINES

be determined from the moiré pattern if the actual loaded model and master grid are available. Differentiating Eq. 1 leads to

$$\frac{d(\tan\phi)}{d\theta} = \frac{1-\frac{p'}{p}\cos\theta}{\left(\cos\theta-\frac{p'}{p}\right)^2} \quad \ldots\ldots\ldots\ldots (38)$$

Because the denominator of Eq. 38 cannot be negative, the sign of the derivaties is determined by the sign of $1 - [(p'/p)\cos\theta]$. If this expression is negative,

$$\frac{p'}{p} > \sec\theta \geq 1 \quad \ldots\ldots\ldots\ldots\ldots\ldots (39)$$

meaning that ϕ decreases for an increase in θ. If the master grid is rotated in a given direction with respect to the model and the fringes rotate in the same direction, this condition is satisfied and $p'/p > 1$. If the grids were originally identical, this positively indicates tensile strain.

For $1 - [(p'/p)\cos\theta]$ negative the situation is not quite so definite because

$$\frac{p'}{p} < \sec\theta \geq 1 \quad \ldots\ldots\ldots\ldots\ldots\ldots (40)$$

can be satisfied in a number of ways when θ is a large angle. If, however, ϕ is not near 90° and the fringes rotate opposite to the rotation of the master grid p'/p may ordinarily be considered to be less than 1, indicating compression for originally identical grids.

Other guides to the sign of $1 - (p/p')$ are sometimes available directly from a moiré photograph. If ϕ is 90° at any point, $p/p' > 1$ from Eq. 17. Once a fringe is known to represent $p/p' > 1$ at any point, the same fringe cannot represent $p/p' < 1$ without going beyond 90°, actually through $\phi = \pi/2 + \theta/2$.

Fringes parallel to the master grid lines represent the condition of no rotation (Eq. 11). Unless they are continuations from areas where the p/p' condition can be evaluated, it is impossible to distinguish from a photograph alone whether p/p' is greater than or less than unity.

USE OF THE BASIC RELATIONSHIPS IN A TWO-DIMENSIONAL STRAIN ANALYSIS

In order to determine strains and rotations associated with two coordinate directions in an actual model, it will obviously be necessary to have models with grid lines perpendicular to these directions. If the model is not identical when turned 90°, two models must be equipped with grids, or, alternatively, two sets of grid lines can be placed on the same model and analyzed separately with a one-way master grid.

Individual measurements of the distance between two fringes cannot be very accurate, as will be apparent from an examination of Figs. 10 and 11. Also, the point being examined may not be exactly on a fringe centered between two fringes.

It is much more convenient and accurate to measure across a series of fringes along a line including the point of interest and plot the accumulated fringe distances from any convenient point as in Fig. 12. A smooth curve is drawn through the plotted points, and the slope of this curve at any point gives fringes per inch, the reciprocal of which is the value in inches per fringe of δ, δ_r, or δ_s as the case may be. In Fig. 12(b) because there is no rotation along an axis of symmetry, the process of differentiation gives the true strain directly.

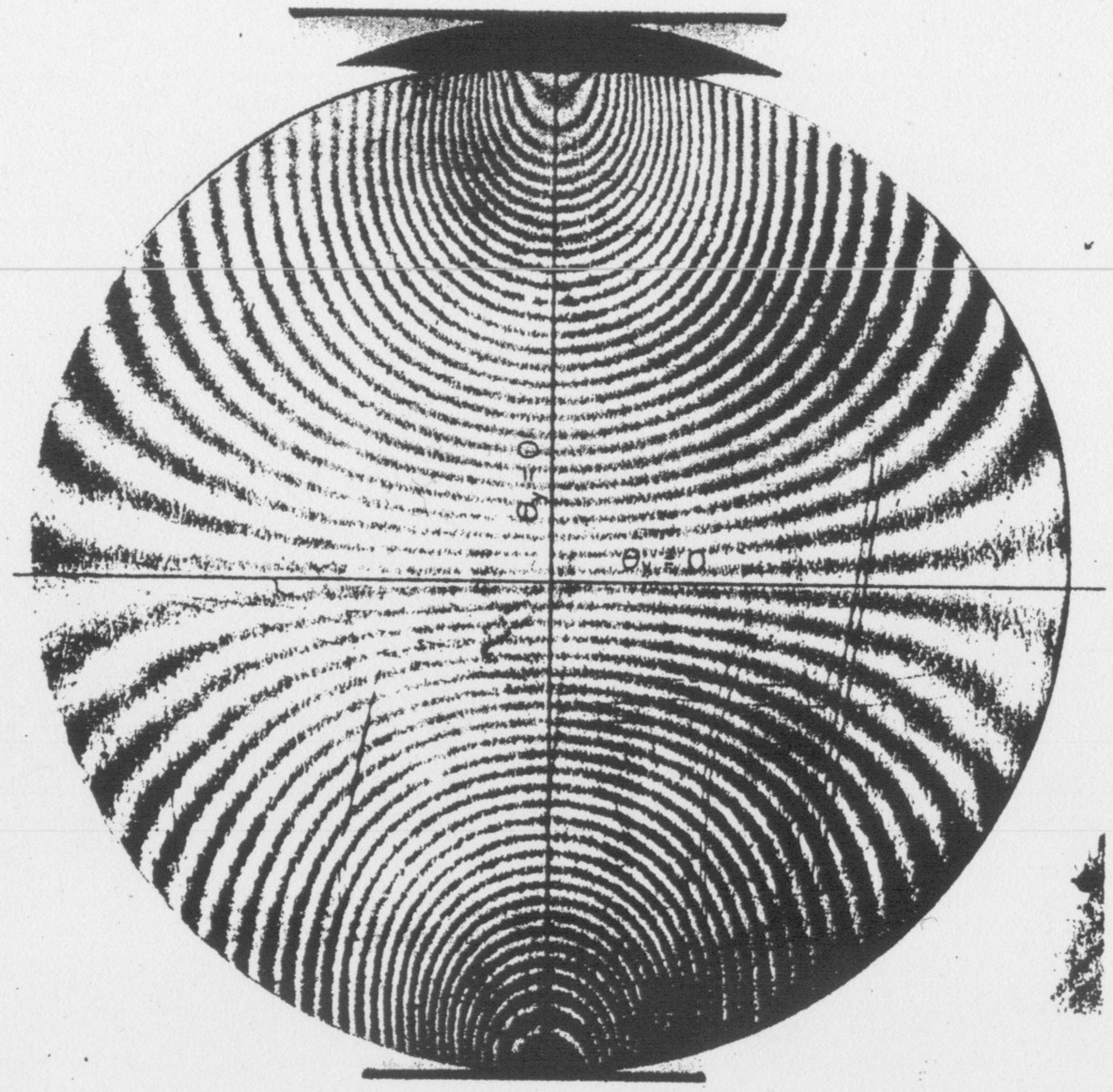

FIG. 10.—MOIRÉ FRINGES ON DISK OF HYSOL 8705 UNDER VERTICAL DIAMETRAL COMPRESSION WITH HORIZONTAL GRIDS (GRIDS = 300 LINES PER INCH ON 4-IN.-DIAMETER DISK)

As will be apparent from Figs. 10 and 11, even in a simplified case such as a disk, it will not usually be possible to measure both δ_r and δ_s at the same point with anything approaching accuracy, and at some points neither can be measured. However, δ can always be measured and values of $1-(p/p')$ and θ from measurements of δ can supplement or check those from measurements of δ_r and δ_s.

The measurements of ϕ will, in general, not be very accurate. However, since one can usually make a choice from among the measurements of δ, δ_r,

and δ_s at any given point of interest, the sensitivity to errors in measurements of ϕ can be kept at a fairly low level for most fringe configurations.

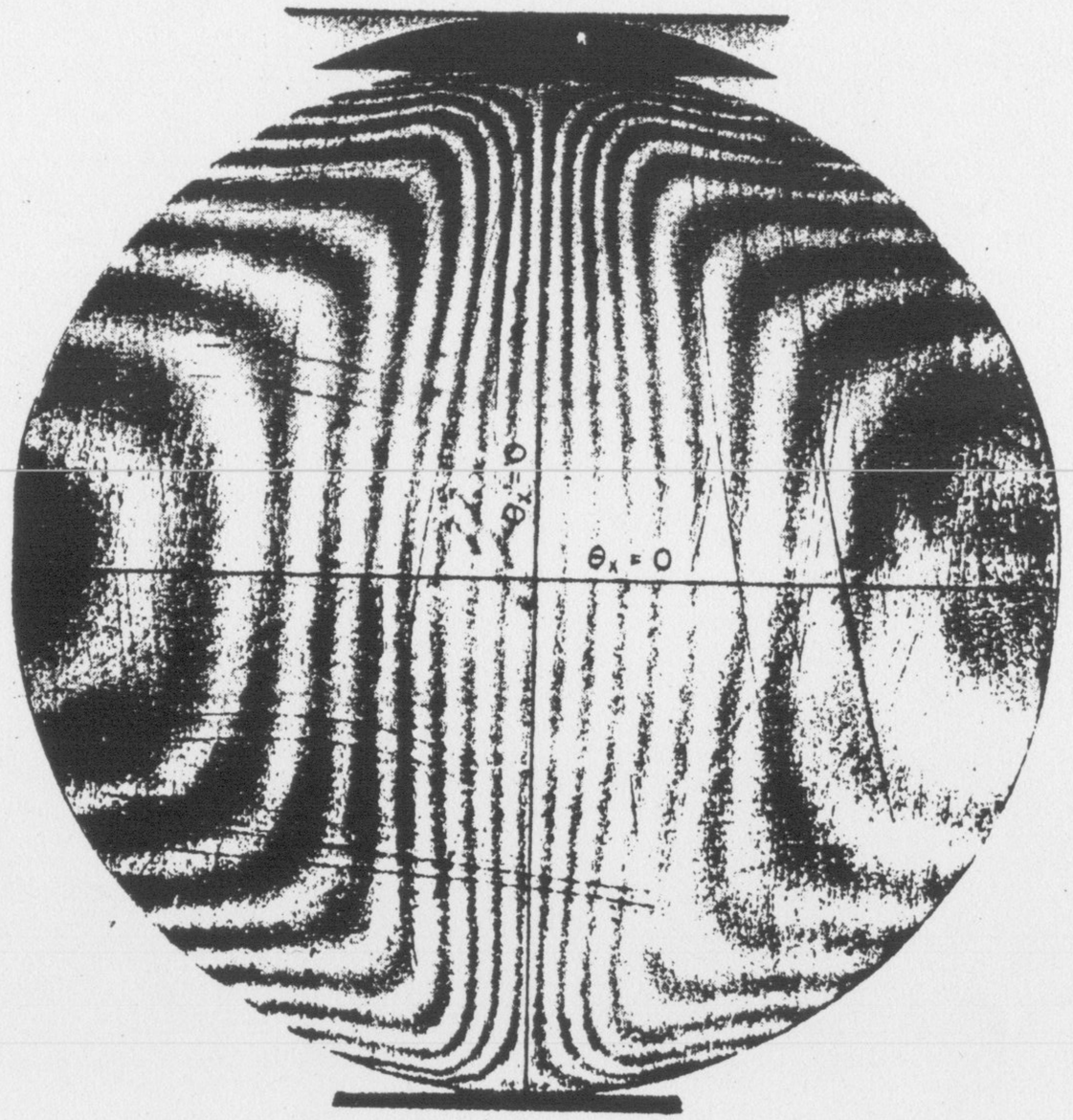

FIG. 11.—MOIRÉ FRINGES ON DISK OF HYSOL 8705 UNDER VERTICAL DIAMETRAL COMPRESSION WITH VERTICAL GRIDS (GRIDS = 300 LINES PER INCH ON 4-IN.-DIAMETER DISK)

The values of $1-(p/p')$ and θ found with grids in each of the two directions comprise all the information needed to solve the general strain problem. In addition to the normal true strains:

$$\epsilon_{x\ \text{true}} = \beta_i \frac{p}{\delta_i} \quad \ldots\ldots\ldots\ldots\ldots\ldots \quad (41a)$$

with grid lines in the y-direction, and

$$\epsilon_{y\ \text{true}} = \beta_i \frac{p}{\delta_i} \quad \ldots\ldots\ldots\ldots\ldots\ldots \quad (41b)$$

with grid lines in the x-direction.

Their nominal (conventional) strain counterparts are

$$\epsilon_{x\ nom} = \frac{\beta_i \frac{p}{\delta_i}}{1 - \beta_i \frac{p}{\delta_i}} \quad \ldots\ldots\ldots\ldots\ldots (42a)$$

with grid lines in the y-direction, and

$$\epsilon_{y\ nom} = \frac{\beta_i \frac{b}{\delta_i}}{1 - \beta_i \frac{p}{\delta_i}} \quad \ldots\ldots\ldots\ldots\ldots (42b)$$

with grid lines in the x-direction. In the foregoing β_i refers to β_δ, β_r or β_s and δ_i refers to the corresponding δ, δ_r, or δ_s.

We have also the rotations

$$\theta_y = \text{arc tan } \frac{\alpha_\delta\, p}{\delta} \quad \ldots\ldots\ldots\ldots\ldots\ldots\ldots (43a)$$

$$\theta_y = \text{arc sin } \frac{\alpha_r\, p}{\delta_r} = \text{arc sin } \frac{\alpha_s\, p}{\delta_s} \quad \ldots\ldots\ldots (43b)$$

with grid lines in the y-direction, and

$$\theta_x = \text{arc tan } \frac{\alpha_\delta\, p}{\delta} \quad \ldots\ldots\ldots\ldots\ldots\ldots\ldots (44a)$$

$$\theta_x = \text{arc sin } \frac{\alpha_r\, p}{\delta_r} = \text{arc sin } \frac{\alpha_s\, p}{\delta_s} \quad \ldots\ldots\ldots (44b)$$

with grid lines in the x-direction.

In general, there will be a rigid body rotation, and if signs are given to θ_x and θ_y (say + for counterclockwise), the rigid rotation ψ will be:

$$\psi = \frac{1}{2}(\theta_x + \theta_y) \quad \ldots\ldots\ldots\ldots\ldots\ldots (45)$$

and the shear strain γ will be:

$$\gamma = \frac{1}{2}(\theta_x - \theta_y) \quad \ldots\ldots\ldots\ldots\ldots\ldots (46)$$

APPLICATION OF THE METHOD TO AN ACTUAL PROBLEM

The moiré method has been applied to the familiar case of a circular disk under diametral compression. In order to obtain a satisfactory level of response with the 300-lines per in. grid available, a sheet was made of urethane rubber (Hysol 8705) on which the grid was photoprinted using the sensitized resist marketed as Gaco. After printing, a 4-in. disk was machined from the 1/2-in.-thick sheet.

The disk was loaded between flat plates, first with grid lines perpendicular to the loading directions (Fig. 10), then with the grid lines parallel to the loading direction (Fig. 11). Photography was by the double-exposure method, the unloaded and loaded conditions being successively exposed on the same sheet of Kodalith film with no intermediate change except for application of the load. (In this method of fringe formation the film-and-lens system must be capable of clearly resolving the individual grid lines at high contrast.)

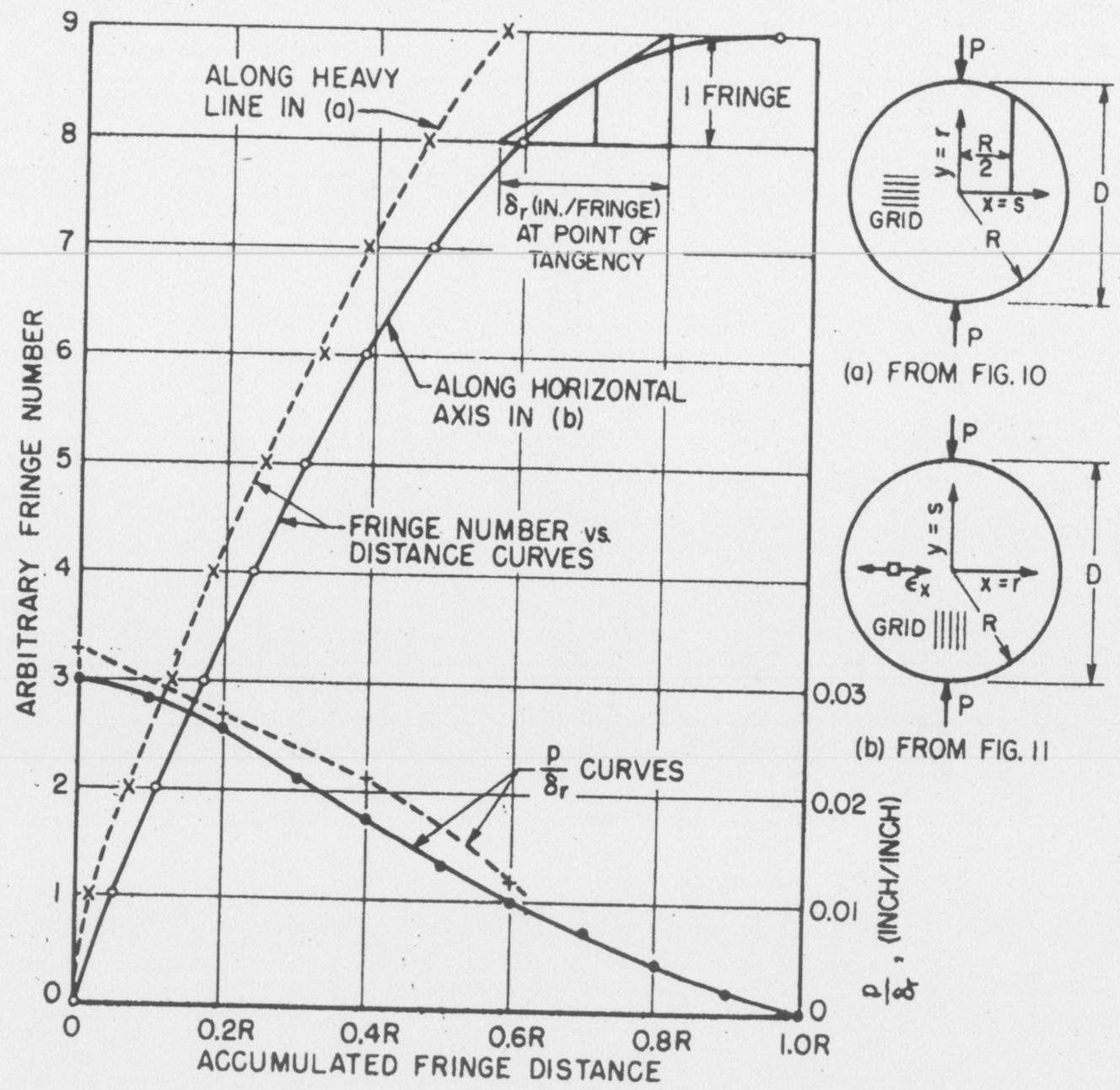

FIG. 12.—DETERMINATION OF δ_r AT ALL POINTS ALONG LINES BY MEANS OF A PLOT OF ACCUMULATED FRINGE DISTANCE FROM ANY ARBITRARY BEGINNING

Fig. 12 is a plot of the measured positions of successive fringes along two representative lines where δ_r could be successfully measured in Figs. 10 and 11. On a separate scale in Fig. 12 are also plotted the values of the quantity p/δ_r determined by differentiation of the fringe-position curves. From the values of p/δ_r (also p/δ_s and p/δ from separate measurements in appropriate directions), the strains can be found as previously described.

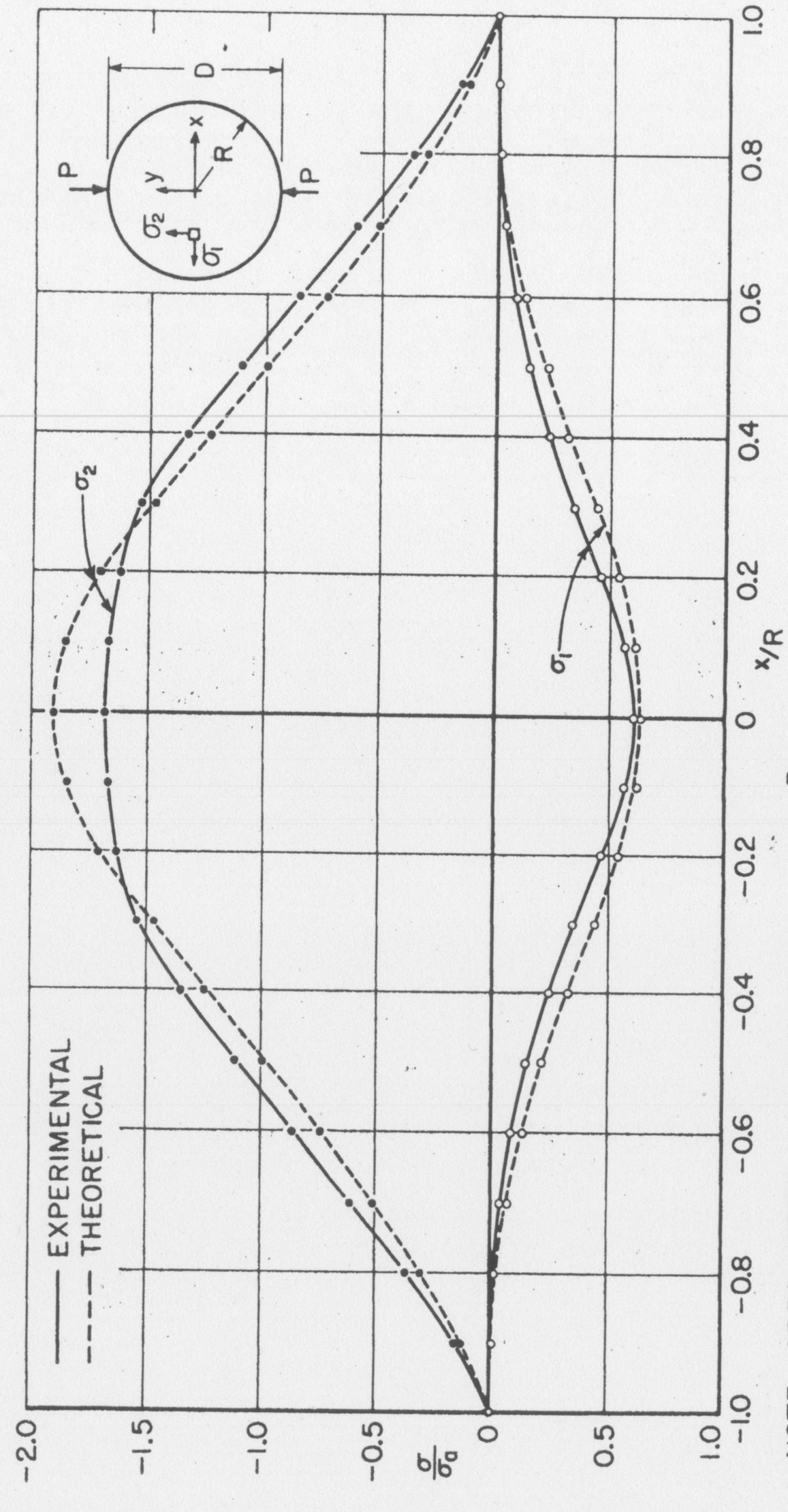

FIG. 13.—PRINCIPAL STRESSES ON THE HORIZONTAL AXIS OF A DISK (HYSOL 8705) UNDER DIAMETRAL COMPRESSION, OBTAINED USING THE MOIRÉ METHOD

From a series of measurements across the horizontal axis of Fig. 10, the value of $\epsilon_{y\ true}$ was determined at a number of points. These values, combined with those for $\epsilon_{x\ true}$ from Fig. 12 and with the modulus of elasticity (also determined by the moiré method), allowed computation of σ_x and σ_y (σ_1 and σ_2 respectively in this case), the results of which are shown in Fig. 13. Also shown in Fig. 13 are the results of a theoretical analysis of the disk when subjected to concentrated loads. The difference between the theoretical and experimental curves can be attributed mainly to the flattening of the disk by the flat plates used to apply the load.

ACKNOWLEDGMENTS

The writers wish to acknowledge the financial support received from the National Science Foundation and from the Armour Research Foundation of the Illinois Institute of Technology.